

# Single Image Haze Removal using a Generative Adversarial Network

Bharath Raj N.

Dept. of Electronics and Communication Engineering,  
Sri Sivasubramaniya Nadar College of Engineering.

Venkateswaran N.

Dept. of Electronics and Communication Engineering,  
Sri Sivasubramaniya Nadar College of Engineering.

## Abstract:

*Single image haze removal is an under constrained problem due to lack of depth information. It is usually performed by estimating the transmission map directly or by using a prior. Other methods use predictive models to estimate the transmission map and perform guided dehazing. In this paper, we propose a conditional GAN, that can directly remove haze from an image, without explicitly estimating transmission map or haze relevant features. We find that, only one module, comprising of the generator and discriminator is enough. We replaced the classic U-Net with the Tiramisu model, yielding much higher parameter efficiency and performance. We also observe that performance during inference is dependent on the diversity of the dataset used for training. Experiments on synthetic and real world hazy images prove that our model performs competitively with the state of the art models.*

**Keywords:** Dehazing; GAN; U-Net; Deep Learning

## Introduction:

Haze is a natural phenomenon caused due to particles in the atmosphere absorbing and scattering light. Due to this, in a hazy atmosphere, light emanating from distant sources are often scattered, and the observer perceives a reduction in contrast. Moreover, images with haze have reduced visibility and color fidelity. Because of this, haze removal is highly sought after where loss in contrast and visibility is of prime importance, such as autonomous vehicles. It is also highly desired in photography and other computer vision applications.

For visual comparison, **Figure 1** shows a hazy image on the left, and its haze-free counterpart on the right.



**Fig. 1:** Sample dehazing results using the proposed method. Left: Input hazy image, Right: Output dehazed image.

Clearly, the amount of degradation is significant, and several methods have been proposed to extract the haze-free image.

Consider a hazy scene being pictured with a camera. The scattered light (Airlight) blends with the image signal and causes a shift in the apparent brightness and colour of the scene. Furthermore, the signal received by the camera from the scene point, gets attenuated along the line of sight. The amount of degradation increases with depth. The image degradation can be modelled as an additive combination of the factors defined above:

$$I(x) = J(x)t(x) + A(x)(1 - t(x)) \quad (1)$$

The first term represents the Direct Attenuation, and the second term represents the Airlight. Here,  $x$  is the pixel coordinates in the image.  $I(x)$  represents the hazy image,  $J(x)$  is its haze-free counterpart and  $t(x)$  is the transmission map [22]. The term  $A(x)$  is the global atmospheric light. When atmospheric light is homogeneous, the transmission map is given by:

$$t(x) = e^{-\beta d(x)} \quad (2)$$

Here,  $\beta$  refers to the attenuation coefficient and  $d(x)$  refers to the scene depth. By estimating the transmission map, we can recover the original haze-free image using:

$$J(x) = \frac{I(x) - A(x)(1 - t(x))}{t(x)} \quad (3)$$

Accurate, straightforward recovery of the transmission map requires depth information. Several dehazing algorithms have obtained depth information by considering multiple images of the same scene, 3D modelling or images in different polarizations [23,34,25].

Single Image dehazing is an under constrained problem. Classical single image dehazing algorithms are dependent on the assumption of a good prior. Accordingly, several methods have been proposed for dehazing using priors [1, 4]. But, the performance of these algorithms depend upon the accuracy of the priors, and they often fail to generalize for all types of scenes.

Another class of single image dehazing algorithms are based on statistical machine learning algorithms [5,7,8]. They try to estimate the transmission map or haze relevant features directly, without assuming a prior, and then apply equation (3) to get the haze-free image. Since these methods do not require a manually calculated prior, they often generalize to a broader number of scenes. On the other hand, these algorithms use Euclidean loss to estimate the transmission map, which is prone to artefacts. Guided filtering is usually used to remove some of the artefacts. Moreover, some manually calculate the haze-free image, based on equation (3). This may lead to dips in performance due to the assumptions involved.

To overcome some of these limitations, [8] jointly estimates the transmission map and haze relevant features and then they perform guided dehazing. The method utilizes three modules of U-Net encoder-decoder structures. The first one is a conditional GAN, which

estimates the transmission map. Another U-Net estimates the haze-relevant features. The outputs of both modules are concatenated and is used to perform guided dehazing, eliminating the need of using equation (3). They also use a dataset where the atmospheric light and scattering coefficient were sampled from a range of values, rather than setting it to a constant.

We propose a method to dehaze images using a single neural network module, comprising of a conditional GAN, which directly translates a hazy image to its haze-free counterpart, without any additional information or modules. This model is end to end trainable, and its novel features are listed below.

### Contributions:

- We observe that multiple modules of U-Nets (As in [8]) are not strictly necessary, and a single conditional GAN can perform the necessary functions to remove haze all by itself. The performance is merely dependent on the dataset used for training. Hence, we propose a single-module conditional GAN, that directly translates a hazy image to a haze-free image.
- We replace the conventional U-Net by the 54-Layer Tiramisu. The latter is extremely parameter efficient, and has state of the art performance in semantic segmentation [13].
- We use the Patch Discriminator, as used in [11], to reduce artefacts
- We use a smooth L1 Loss and Perceptual Loss, which are weighted and added to the standard conditional GAN loss.
- We observe that the performance is dependent on the diversity in the input data during training, and we work on that issue by synthetically generating realistic hazy images of indoor and outdoor scenes.

### Related Work:

In this section, we present a brief review on existing literature about dehazing, conditional GANs, loss functions and encoder-decoder architectures.

## A. De-Hazing

Classic haze removal requires us to provide the depth information of the image, so that the transmission coefficient can be calculated at every pixel. A transmission map is hence obtained, and is used to recover the original RGB image by using equation (3). Kopf et. al [23] did this by calculating the depth from multiple images, or a 3D model.

Single image dehazing is under-constrained, as we do not have additional depth information. Several approaches under this domain involve the creation of an image prior, based on certain assumptions. Most of these approaches work locally, on patches of the image, with maybe prone to artefacts. They apply guided filtering to smoothen and reduce such artefacts.

Tan [4] observes that, haze-free images must have higher contrast than its hazy counterpart, and attempts to remove haze by maximizing the local contrast of the image patch. He et. al. [1] found that most patches have pixels that have a very low intensity in at least one color channel. In its hazy counterpart, the intensity of the pixel in that channel is mostly contributed by airlight. Using this information, a dark channel prior is calculated, and is used for dehazing as well as estimating the transmission map of the image. The drawback is that, removing haze from regions which naturally have high intensity, such as the sky, is error prone. Improving on that, Meng et. al [3] imposed boundary constraints on the transmission function to make the transmission map prediction more accurate. Berman et. al [6] suggested a Non-local approach to perform dehazing. They observed that colours in a haze-free image can be approximated by a few 100 distinct colours that form clusters in the RGB space. They find that pixels in an hazy image can be modelled as lines in the RGB space (haze lines), and using this, they estimate the transmission map values at every pixel.

All of these methods are based on one or more key assumptions, which exploit haze relevant features. Some of these assumptions do not hold true in all possible cases. A way to circumvent this issue is to use

deep learning techniques, and let the algorithm decide the relevant features. DehazeNet is a CNN that outputs a feature map, from which the transmission map is calculated [5]. Going a step further, Ren et. al [7] have calculated the transmission map using a multiscale deep CNN.

Generative Adversarial Networks, introduced by Ian Goodfellow et. al [18] can generate an output distribution given a noise distribution as an input. Conditional GANs [11] have the noise distribution conditioned on the input image. They have proved to be immensely effective in several image translation applications such as Super Resolution, De-Raining, and several others [9,10].

[8] uses three modules of U-Net neural networks, to perform guided dehazing of an image. The first module is a conditional GAN, trained with Adversarial loss added to Euclidean loss, to estimate the transmission map. The second module estimates the haze relevant features, and is concatenated with the transmission map. Finally, the third module translates this concatenated combination to obtain a haze-free image, trained with Euclidean and Perceptual Loss.

## B. Loss Functions

The conditional GAN loss function is shown below, as defined in [11]:

$$Loss_{CGAN} = \mathbb{E}_{(x,y)}[\log(D(x,y))] + \mathbb{E}_{(x,z)}[\log(1 - D(x, G(x,z)))] \quad (4)$$

Here, D refers to the discriminator and G refers to the generator. The input image is defined as  $x$ , and its corresponding target is defined as  $y$ . The generator tries to output an image, given a random noise vector  $z$ , conditioned on the input image  $x$ . The noise vector is added to improve the stochasticity of the model. Instead of that, in [11] they used noise in the form of dropout applied to the layers of the generator.

In the equation,  $D(x, y)$  is the expected discriminator output when it is shown the input image  $x$ , and the target image  $y$ , concatenated along the channel axis. This

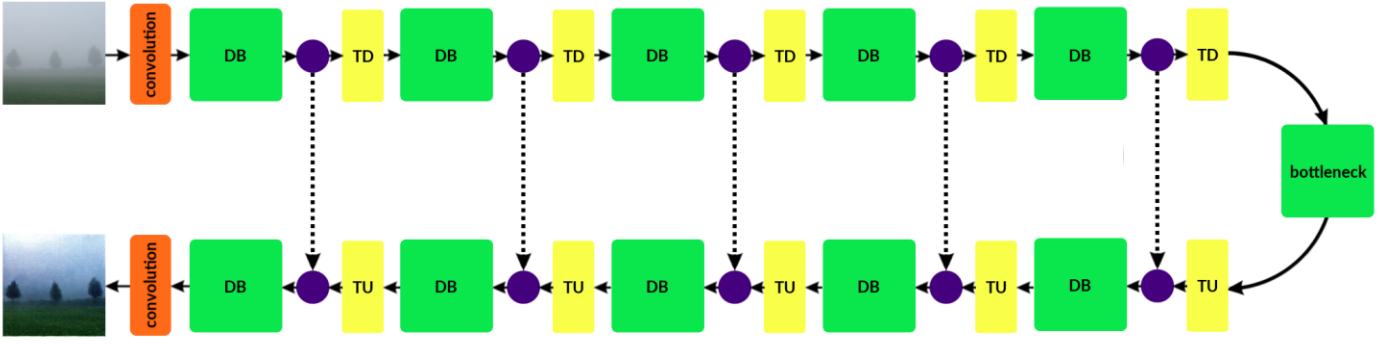


**Fig. 2: Generator** of the proposed model. It consists of **Dense Blocks** (DB), **Transition Down layers** (TD), **Transition Up layers** (TU) and a **Bottleneck layer**. Additionally, it contains an **input convolution** and an **output convolution**. Dotted lines imply a **concatenation operation**. The components are further elucidated in Fig. 3 and Table 1.

value must be maximized. Similarly,  $D(x, G(x, z))$  is the expected discriminator output when it is shown the input image  $x$ , and the generated image  $G(x, z)$ , concatenated along the channel axis. This value must be minimized. Hence, the discriminator's parameters are modified such that  $Loss_{CGAN}$  is maximized. Similarly, the generator must minimize the second term in the equation. Overall, the optimization objective can be given as described below:

$$G^* = \arg \min_G \max_D Loss_{CGAN} \quad (5)$$

In addition to the GAN loss function shown above, research has shown that adding L2 [20] or smooth L1 loss [11] would improve the image quality. L2 Loss is more susceptible to artefacts than the smooth L1 Loss [11].

Certain image translation methods using conditional GANs such as [10] have shown that using the Feature Reconstruction Perceptual Loss [12] provides a much visually pleasing result. The target and the generated image are passed through a VGG net [19], and the L2 Loss between the feature maps produced after the Pool-4 layer is computed.

### C. Encoder-Decoder Architecture

It is noted that, in several image translation problems [9,10], an encoder-decoder architecture is used as the generator. The encoders layers typically have convolution-batchnorm-relu operations. The image is progressively downsampled until a bottleneck layer, after which the process is reversed to obtain the output image. In typical image translation problems, the output and input share a lot of structural information. It would be beneficial to share this information directly across the network, which is done using skip connections. This gives us the U-Net Architecture.

Recently, the DenseNet architecture was introduced, and it had achieved comparable or better results in image classification problems, using lesser parameters than its competitors [14]. The core component of the DenseNet is the dense block, which concatenates every layer's output with its input, and feeds it to the next layer. This enhances information and gradient flow. It was also found that applying non-linearities and activations before applying the convolution operation proved to be crucial. The One Hundred Layer Tiramisu architecture is similar to the U-Net architecture, except that it uses dense blocks. It was shown that they obtained a good boost in performance, while being extremely parameter efficient. [13]

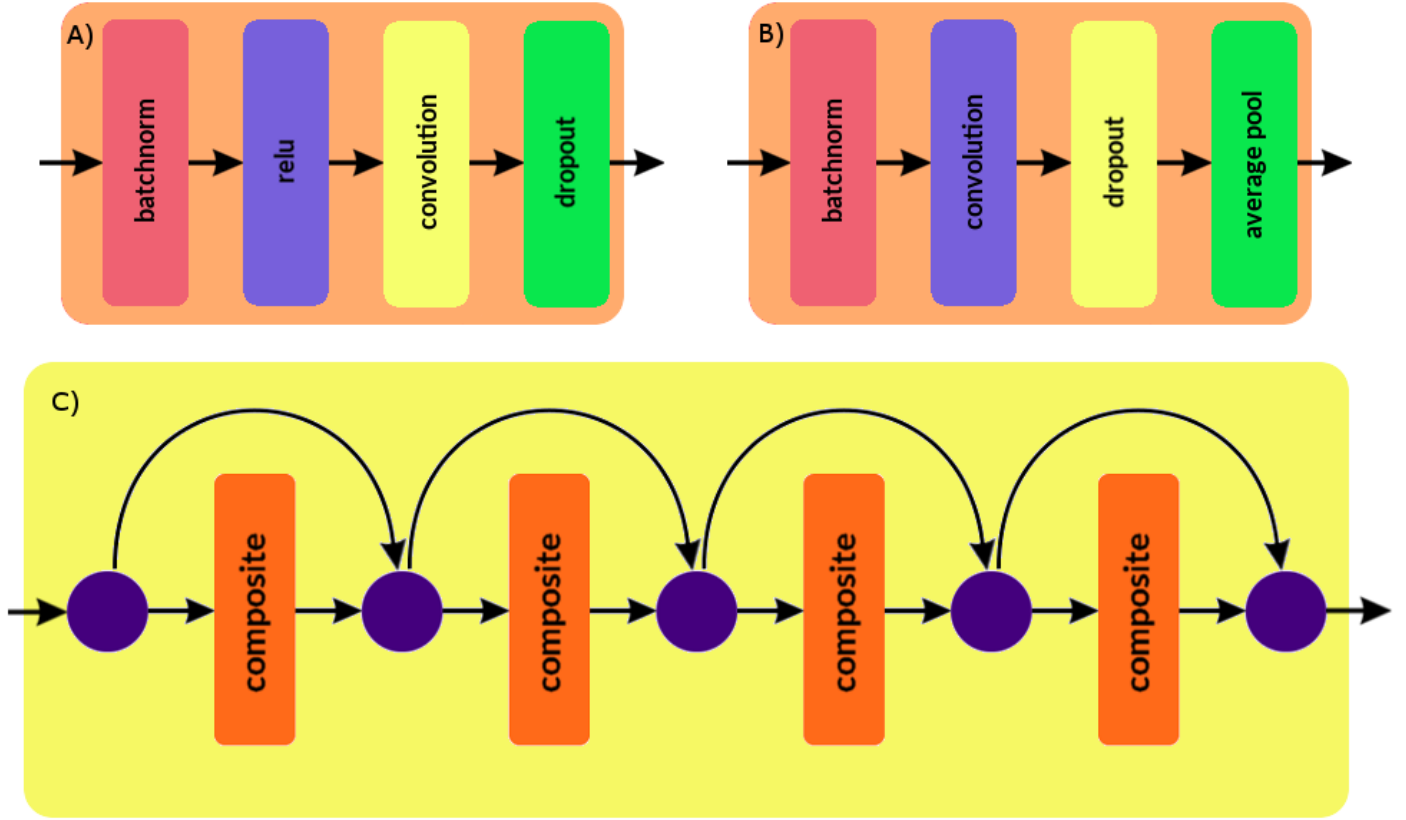


**Fig. 3:** Expanded view of the various components of the generator. **A: Transition Down (TD) layer;** **B: Composite Layer** (within a dense block); **C: Dense Block** with 4 composite layers. Curved lines ending on purple dots imply a concatenation operation. The Transition Up layer comprises only of a transpose convolution operation, and hence not shown here.

### Proposed Model:

In this paper, we introduce a single, end to end trainable, conditional Generative Adversarial Network, which is capable of removing haze without estimating the transmission map explicitly. The components of the network is described in the following subsections.

#### A. Generator

We replace the conventional U-Net used as the generator, with the 54 Layer Tiramisu [13]. This enhances information and gradient flow, due to the presence of dense blocks [14]. The model has 5 Dense Blocks on the encoder side, 5 Dense Blocks on the decoder side and one Dense Block as the bottleneck layer. On the encoder side, each Dense Block is followed by a Transition Down (TD) Layer. The TD Layer comprises of (BatchNorm-Relu-Convolution) operations.

Similarly, on the decoder side, each Dense Block is followed by a Transition Up (TU) Layer. The TU Layer has only a Deconvolution operation. Each Dense Block in the encoder and the decoder has 4 layers each. The Dense Block in the bottleneck has 15 layers. The growth rate is fixed at 12. A detailed description of the architecture is given in **Table 1**.

The spatial dimensions of the images are halved after passing through a Transition Down layer, and doubled after passing through a Transition Up layer. Compared with the vanilla U-Net, there is a massive reduction in the number of trainable parameters for the generator (1M parameters).

#### B. Discriminator

We use the same discriminator network (Patch GAN) as used in the original conditional GAN paper [11]. This

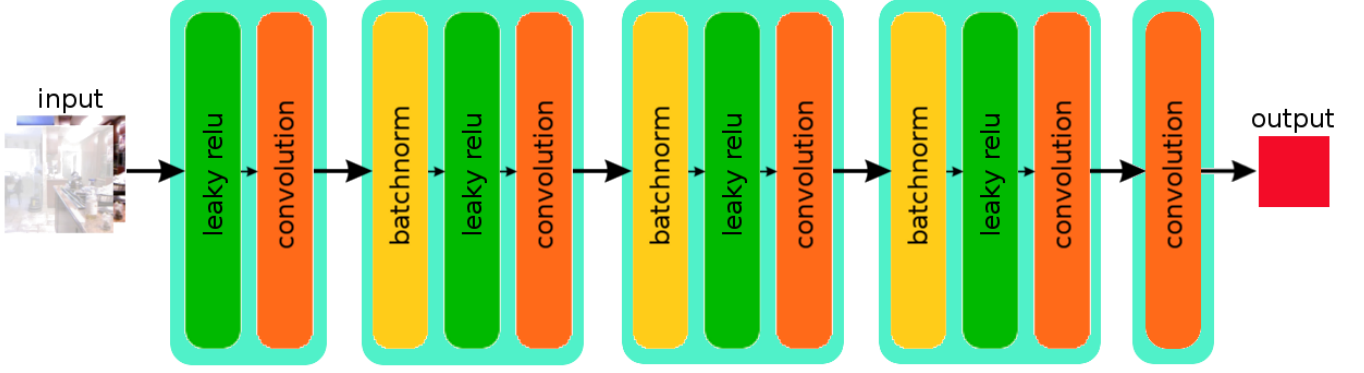


**Fig. 4: Discriminator** of the proposed model. It takes in an input of an hazy image concatenated with the ground truth or the generated image. It outputs a 30x30 matrix, which is used to test if the image is real or fake.

network performs patch-wise comparison of the target and generated images, rather than pixel-wise comparison. This is enabled by passing the images through a CNN, whose receptive field at the output is larger than one pixel (i.e. corresponds to a patch of pixels in the original image). Valid padding is used to control the effective receptive field. We follow the 70x70 patch discriminator, as described in the Pix2Pix GAN paper [11]. We apply pixel-wise comparison at the last set of feature maps. The effective receptive field at the feature map is larger than a pixel, and hence it covers a patch of the images. This removes a good amount of artefacts in the images. [11]

### C. Loss Functions

The loss function that we use to optimize our network has three components, which are weighted and added to give the Total Loss ( $Loss_{total}$ ). The Total Loss is given by:

$$Loss_{total} = W_{gan} * L_{Adv} + W_{L1} * L_{L1} + W_{vgg} * L_{vgg} \quad (6)$$

The corresponding loss components are described as follows:

#### Adversarial Loss

The conditional GAN loss is defined as below:

$$L_{Adv} = \mathbb{E}_{(x,y)}[\log(D(x,y))] + \mathbb{E}_{(x,z)}[\log(1 - D(x, G(x,z)))] \quad (7)$$

As mentioned in the earlier section, **D** refers to the discriminator and **G** refers to the generator. The input hazy image is defined as **x**, and its corresponding haze free counterpart is defined as **y**. We follow the method used in [11], to use dropout as our source of noise. In our model, we perform one generator update, followed by one discriminator update per iteration. The result is multiplied with a scalar weight  $W_{gan}$  and is added to the total loss.

#### Smooth L1 Loss

As stated in [11], using a weighted L1 Loss along with the adversarial loss reduced artefacts in the output image. The L1 Loss between the target image **y** and the generated image  $G(x, z)$  is calculated as follows::

$$L_{L1} = \mathbb{E}_{x,y,z}[\|y - G(x, z)\|_1] \quad (8)$$

The result is multiplied with a scalar weight  $W_{L1}$  and is added to the total loss.

#### Perceptual Loss

As used in the following papers [9,10], we added the feature reconstruction perceptual loss to our total loss. The generated and target images are passed through a non-trainable VGG-19 network. The L2 Loss of the outputs of the two images, after passing through the Pool-4 layer is calculated. The perceptual loss is defined as follows:



$$L_{vgg} = \frac{1}{CWH} \sum_{c=1}^C \sum_{w=1}^W \sum_{h=1}^H \|V(G(x, z)^{c,w,h}) - V(y^{c,w,h})\|_2^2 \quad (9)$$

Here, C,W,H represents the output's channels, width and height respectively. This value is a constant, and for the output of the Pool-4 layer, it can approximated to  $1e-5$ . V represents the non-linear CNN transformation, which is performed by the VGG network. The result is multiplied with a scalar weight  $W_{vgg}$  and is added to the total loss.

| Generator     |              |
|---------------|--------------|
| Operation     | Output Shape |
| Input Conv    | 256,256,48   |
| DB Encoder 1  | 256,256,96   |
| TD 1          | 128,128,48   |
| DB Encoder 2  | 128,128,96   |
| TD 2          | 64,64,48     |
| DB Encoder 3  | 64,64,96     |
| TD 3          | 32,32,48     |
| DB Encoder 4  | 32,32,96     |
| TD 4          | 16,16,48     |
| DB Encoder 5  | 16,16,96     |
| TD 5          | 8,8,48       |
| DB Bottleneck | 8,8,228      |
| TU 5          | 16,16,48     |
| DB Decoder 5  | 16,16,192    |
| TU 4          | 32,32,48     |
| DB Decoder 4  | 32,32,192    |
| TU 3          | 64,64,48     |
| DB Decoder 3  | 64,64,192    |
| TU 2          | 128,128,48   |
| DB Decoder 2  | 128,128,192  |
| TU 1          | 256,256,48   |
| DB Decoder 1  | 256,256,192  |
| Output Conv   | 256,256,3    |
| Discriminator |              |
| Operation     | Output Shape |
| Layer 1       | 128,128,64   |
| Layer 2       | 64,64,128    |
| Layer 3       | 32,32,256    |
| Layer 4       | 31,31,512    |
| Layer5        | 30,30,1      |

**Table 1:** Output shapes of the images when passed through each component of the generator and discriminator. Input shapes are 256,256,3 for generator and 256,256,6 for the discriminator.

## Experiments

### A. Dataset:



**Fig. 5:** Sample indoor and outdoor images from **Dataset-C**. Left: Synthetically added hazy image. Right: Ground Truth.

We observe that performance of the model heavily depends on the type of data used for training. We investigated the same using three different datasets. All images were resized to the size (256,256,3).

We first investigated the our model's performance, when trained on images with synthetically added haze, without depth information. We used the smaller version images (256x256) from the MIT Places 365 Standard dataset [17]. A set of 2300 images for training and 624 images for testing were randomly sampled from the dataset. The transmission coefficient (t) was given a random value, sampled from the uniform distribution [0.3, 0.5]. The value is constant throughout the image. Atmospheric light (A) was set to 1, and homogenous fog was added using equation (1). Let us call this Dataset-A.

To create a realistic haze dataset, we need depth information. Since it is difficult to find a large, realistic haze/ground-truth image pair dataset, we synthetically created one, using the NYU Depth Dataset [2]. The

dataset comprises of 1449 indoor scenes and their corresponding RGB-D pair. We wanted to simulate images with heavy haze/fog, and hence we initially sample a base value for the transmission coefficient, from the uniform distribution [0.2, 0.4]. The transmission map ( $t$ ) for the images were created using the RGB-D images, and then was scaled by the previously sampled value, to obtain the transmission coefficient at every point in the image. Atmospheric light ( $A$ ) is set to 1 as before used to add homogeneous fog to the images equation (1). Let us call this Dataset-B.

We noted that the NYU Depth Dataset had only indoor scenes. Certain features such as the sky are a distinct feature of outdoor scenes, and are not found in the above dataset. Such additional information could improve performance. To address the same, we used the Make 3D [20, 21] dataset to generate outdoor haze/ground-truth image pairs. The images and depth maps were resized and haze/fog was added using the same method as described for Dataset-B. We then merged these new images with Dataset-B to create Dataset-C. The dataset had a total of 1776 images, of size (256,256,3).



**Fig. 6:** Comparing the effects of different datasets on the results. The images on the left are real life hazy images. In the top row, the second image was dehazed by a model trained on Dataset-A, whereas the third image was dehazed by a model trained on Dataset-C. In the bottom row, the second image was dehazed by a model trained on Dataset-B, whereas the third image was dehazed by a model trained on Dataset-C.

We trained our model on each of these datasets. The performance varies with respect to the dataset used, as

expected. Figure 6 compares the results obtained from models trained using each of the three datasets. As we can see from the first row of Figure 6, performance by training on Dataset-A is not as good as Dataset-B or C when dealing with images with heavy haze. And from the second row of Figure 6, performance by training on Dataset-B, which purely has indoor images (Limited information about natural outdoor colors), has slightly worse performance than Dataset-C. This could be attributed to the fact that the network trained using Dataset-C, learns how to handle images with the sky in the background. It is worth noting that, performance of Dataset-C can also overfit or mode collapse to that of Dataset-B (Since Dataset-C has all the images of Dataset-B). But, by using a validation set and a metric (described in the next section), we can save the best model before it starts to behave non-ideally.

## B. Training Details:

The weight values used were  $W_{vgg} = 10$ ,  $W_{gan} = 2$ ,  $W_{L1} = 100$ . The learning rate value was fixed at 0.001. We used the Adam Optimizer to perform gradient descent. The model was coded on python using the TensorFlow framework. It was then trained on a Laptop with Nvidia GTX 950M (2GB) graphics card. It took approximately 1.6s per step with these configurations.

The dataset (Dataset-C) was split into a training set, validation set and a test set. A set of 1550 images were randomly chosen from the dataset, to create the training dataset. Additionally, these images were flipped horizontally and added to the training dataset, creating a total of 3100 images. The images are shuffled every epoch. The remaining 226 images was split into a validation set of 76 images and a test set of 150 images. Due to the rather small size of the dataset, we used a very small validation and test set. Nevertheless, this was sufficient to assess the generalization capability of the model and pick out the best performing model.

We perform one update of the generator followed by one update of the discriminator per iteration. Hence, two global steps are taken per iteration, one for each update. A common issue with conditional GANs is that, it is



| Model | He et. al | Meng et. al | Berman et. al | Proposed Model |
|-------|-----------|-------------|---------------|----------------|
| PSNR  | 13.89     | 14.48       | 12.48         | 20.32          |
| SSIM  | 0.659     | 0.651       | 0.649         | 0.759          |
| Score | 1.354     | 1.375       | 1.274         | 1.775          |

**Table 2:** Results of the quantitative analysis conducted on our test set (Dataset-C). Our synthetic test dataset has 150 images of extremely intensive haze. Our model performs much better as it is trained on similar images, and does not depend on priors.

nearly impossible to tell when to stop training by just looking at the loss graphs. The loss values do not indicate when the best performance has been achieved, and at times the GAN can fall into non-ideal conditions such as mode collapse.

### C. Performance Metrics:

A haze removal algorithm’s performance can be evaluated on several factors, among them, two of the most frequently used factors are the PSNR and SSIM. Peak Signal to Noise Ratio (PSNR) measures the ability of the algorithm to remove noise (haze) from a noisy image. Two identical images will have a PSNR value of infinity. For measuring haze removal capability, a higher PSNR value indicates better performance. Structural Similarity Index Measure (SSIM), measures how similar two images are. Two identical images will have a SSIM of 1.

On the contrary, there’s no guarantee that images with high PSNR will be visually pleasing and images with high SSIM will have a good haze removal quality. Hence, we need a metric that has both properties. We define a metric called score, which is a weighted sum of the PSNR and the SSIM of the image.

$$Score = W_{PSNR} * PSNR + W_{SSIM} * SSIM$$

The PSNR weight ( $W_{PSNR}$ ) is set to 0.05 and the SSIM weight ( $W_{SSIM}$ ) is set to 1. The model is saved whenever the score reaches a higher value in the test set. We save a maximum of 10 checkpoints at any given time. We also verify performance of the top few models by dehazing some real life images with haze.

### D. Quantitative and Qualitative evaluation:

In this section, we given a quantitative and a visual comparison of our model with other popular dehazing techniques. We compare the PSNR and SSIM values obtained by these models on our test set. For our quantitative analysis, the following models are selected:

- Dark channel prior haze removal (He et. al, [1])
- Boundary constraint and context regularization (Meng et. al, [3])
- Non local image dehazing (Berman et. al, [6])

Table 2 lists out the PSNR, SSIM and our score values for the quantitative analysis. Clearly, our model performs really well on our synthetic test dataset. The rather lower score of the other models can be attributed to the fact that our synthetic test dataset has very heavy haze, which may not be in sync with the assumptions taken by the algorithms. Moreover, it reinforces the idea that our model performs very well to undo the synthetic transformation that we applied.

To conclusively prove the effectiveness of our model, we evaluated it on some real world hazy images. Moreover, we compare our results with those of the dehazing methods listed above. In addition to the above, we also include the work done by Zhang et. al [8] and Cai et. al [5] for visual comparison. The original hazy image, along with the dehazed counterparts are illustrated in Fig 7 and Fig 8.

In Figure 7, from the first row of images, it is evident that our algorithm performs really well in extreme haze conditions. It can be seen that our algorithm is able to extract an equal or more amount of detail from the input hazy images than the other methods. This is evident



**Fig. 7:** Visual comparison of dehazing method on real world images.

from the first row and third row of images. The output is also realistic in terms of color. Looking at the images in last row, we also note that the sky has proper color in our dehazed image. This is in contrast to the slight darkening near the horizon with the other methods. Resolution of far off images is also competitive with other methods, as seen from the second and fourth row of images.

In Figure 8, we have more comparisons. From the first set of images it is evident that more details are able to be resolved from hazy images using our method. For instance, the bridge has a better color in our dehazed image. Likewise, from the second set of images we see that minor details of the far off buildings are resolved clearly in our dehazed image.





Input Image

Cai et. al [5]

He et. al [1]

Meng et. al [3]



Berman et. al [6]



Zhang et. al [8]



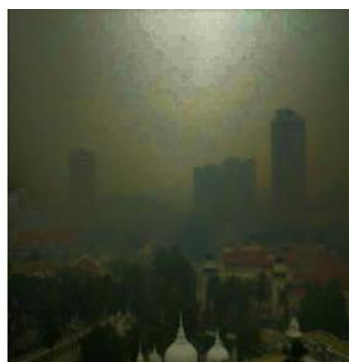
Proposed Model



Input Image



Cai et. al [5]



He et. al [1]



Meng et. al [3]



Berman et. al [6]



Zhang et. al [8]



Proposed Model

**Fig. 8:** Visual comparison of dehazing method on real world images.

## Conclusion:

This paper presented a single module, conditional generative adversarial network, that can directly translate a hazy image into a haze-free image. We increased the parameter efficiency and performance of the model by replacing the U-Net with the Tiramisu model. By using the Patch GAN discriminator and Smooth L1 Loss, we reduced the presence of artefacts significantly. We provided a quantitative and visual comparison of our model with other popular dehazing algorithms, proving the superior quality of our model. However, the size of the input image is restricted (256x256), but further work can be done to make this flexible. Also, larger Tiramisu models can be experimented with.

## References:

- [1] He, Kaiming, Jian Sun, and Xiaoou Tang. "Single image haze removal using dark channel prior." *IEEE transactions on pattern analysis and machine intelligence* 33.12 (2011): 2341-2353.
- [2] Silberman, Nathan, Derek Hoiem, Pushmeet Kohli, and Rob Fergus. "Indoor segmentation and support inference from rgb-d images." In *European Conference on Computer Vision*, pp. 746-760. Springer, Berlin, Heidelberg, 2012.
- [3] Meng, Gaofeng, Ying Wang, Jiangyong Duan, Shiming Xiang, and Chunhong Pan. "Efficient image dehazing with boundary constraint and contextual regularization." In *Computer Vision (ICCV), 2013 IEEE International Conference on*, pp. 617-624. IEEE, 2013.
- [4] Tan, Robby T. "Visibility in bad weather from a single image." In *Computer Vision and Pattern Recognition, 2008. CVPR 2008. IEEE Conference on*, pp. 1-8. IEEE, 2008.
- [5] Cai, Bolun, Xiangmin Xu, Kui Jia, Chunmei Qing, and Dacheng Tao. "Dehazenet: An end-to-end system for single image haze removal." *IEEE Transactions on Image Processing* 25, no. 11 (2016): 5187-5198.
- [6] Berman, D. and Avidan, S., 2016. Non-local image dehazing. In *Proceedings of the IEEE conference on computer vision and pattern recognition* (pp. 1674-1682).
- [7] Ren, Wenqi, Si Liu, Hua Zhang, Jinshan Pan, Xiaochun Cao, and Ming-Hsuan Yang. "Single image dehazing via multi-scale convolutional neural networks." In *European conference on computer vision*, pp. 154-169. Springer, Cham, 2016.
- [8] Zhang, He, Vishwanath Sindagi, and Vishal M. Patel. "Joint Transmission Map Estimation and Dehazing using Deep Networks." *arXiv preprint arXiv:1708.00581* (2017).
- [9] Ledig, Christian, Lucas Theis, Ferenc Huszar, Jose Caballero, Andrew Cunningham, Alejandro Acosta, Andrew Aitken et al. "Photo-Realistic Single Image Super-Resolution Using a Generative Adversarial Network." In *Proceedings of the IEEE Conference on Computer Vision and Pattern Recognition*, pp. 4681-4690. 2017.
- [10] Zhang, He, Vishwanath Sindagi, and Vishal M. Patel. "Image de-raining using a conditional generative adversarial network." *arXiv preprint arXiv:1701.05957* (2017).
- [11] Isola, Phillip, Jun-Yan Zhu, Tinghui Zhou, and Alexei A. Efros. "Image-To-Image Translation With Conditional Adversarial Networks." In *Proceedings of the IEEE Conference on Computer Vision and Pattern Recognition*, pp. 1125-1134. 2017.
- [12] Johnson, Justin, Alexandre Alahi, and Li Fei-Fei. "Perceptual losses for real-time style transfer and super-resolution." In *European Conference on Computer Vision*, pp. 694-711. Springer, Cham, 2016.
- [13] Jégou, Simon, Michal Drozdal, David Vazquez, Adriana Romero, and Yoshua Bengio. "The one hundred layers tiramisu: Fully convolutional densenets for semantic segmentation." In *Computer Vision and Pattern Recognition Workshops (CVPRW), 2017 IEEE Conference on*, pp. 1175-1183. IEEE, 2017.
- [14] Huang, Gao, Zhuang Liu, Kilian Q. Weinberger, and Laurens van der Maaten. "Densely connected convolutional networks." In *Proceedings of the IEEE conference on computer vision and pattern recognition*, vol. 1, no. 2, p. 3. 2017.
- [15] Ronneberger, Olaf, Philipp Fischer, and Thomas Brox. "U-net: Convolutional networks for biomedical image segmentation." In *International Conference on Medical image computing and computer-assisted intervention*, pp. 234-241. Springer, Cham, 2015.
- [16] Long, Jonathan, Evan Shelhamer, and Trevor Darrell. "Fully convolutional networks for semantic segmentation." In *Proceedings of the IEEE conference on computer vision and pattern recognition*, pp. 3431-3440. 2015.
- [17] Zhou, Bolei, Agata Lapedriza, Aditya Khosla, Aude Oliva, and Antonio Torralba. "Places: A 10 million image database for scene recognition." *IEEE transactions on pattern analysis and machine intelligence* (2017).
- [18] Goodfellow, Ian, Jean Pouget-Abadie, Mehdi Mirza, Bing Xu, David Warde-Farley, Sherjil Ozair, Aaron Courville, and Yoshua Bengio. "Generative adversarial nets." In *Advances in neural information processing systems*, pp. 2672-2680. 2014.
- [19] Simonyan, Karen, and Andrew Zisserman. "Very deep convolutional networks for large-scale image recognition." *arXiv preprint arXiv:1409.1556* (2014).
- [20] Saxena, Ashutosh, Sung H. Chung, and Andrew Y. Ng. "Learning depth from single monocular images." In *Advances in neural information processing systems*, pp. 1161-1168. 2006.
- [21] Saxena, Ashutosh, Sung H. Chung, and Andrew Y. Ng. "3-D depth reconstruction from a single still image." *International journal of computer vision* 76, no. 1 (2008): 53-69.

- [22] Fattal, Raanan. "Single image dehazing." *ACM transactions on graphics (TOG)* 27, no. 3 (2008): 72.
- [23] J. Kopf, B. Neubert, B. Chen, M. Cohen, D. Cohen-Or, O. Deussen, M. Uyttendaele, and D. Lischinski. Deep photo: Model-based photograph enhancement and viewing. SIG-GRAPH Asia, 2008.
- [24] S. Shwartz, E. Namer, and Y. Y. Schechner. Blind haze separation. *CVPR*, 2:1984–1991, 2006.
- [25] S. G. Narasimhan and S. K. Nayar. Contrast restoration of weather degraded images. *PAMI*, 25:713–724, 2003.